Gum Arabic as a Binder for Paste Extrusion Additive Manufacturing Using Rice Husks

Beinomugisha Vian
Department of Mechatronics and Mechanical Engineering, Pan African University of Basic Science, Technology and Innovation (PAUSTI), Juja, Kenya
beinomugishavian01@gmail.com (corresponding author)

Samuel Kabini Karanja
Department of Mechatronics Engineering, Jomo Kenyatta University of Agriculture and Technology, Juja, Kenya
kkabini@eng.jkuat.ac.ke

James Wamai Mwangi
Department of Mechatronics Engineering, Jomo Kenyatta University of Agriculture and Technology, Juja, Kenya
jwamai@jkuat.ac.ke

Leif Bretschneider
Institute of Machine Elements, Engineering Design and Manufacturing (IMKF), Technische Universitat Bergakademie Freiberg, Germany
leif.bretschneider@imkf.tu-freiberg.de

Received: 9 January 2026 | Revised: 11 February 2026 and 24 April 2026 | Accepted: 30 April 2026

 DOI: https://doi.org/10.48084/etasr.17432

ABSTRACT

This study evaluates Gum Arabic (GA) powder as a biodegradable binder for rice-husk-based composites fabricated using Material Extrusion with Chemical Reaction Bonding (MEX-CRB). The MEX-CRB technique deposits visco-plastic or bio-based pastes in sequential layers through a nozzle, directed by G-codes derived from STL files. This method enables the processing of materials beyond traditional polymer-based systems and applies to ceramics, biomedical scaffolds, construction, and sustainable manufacturing. MEX-CRB still primarily employs synthetic binders, raising sustainability concerns; therefore, this study investigates GA as an environmentally responsible alternative. The effects of particle size, binder ratio, flowability, rheological properties, drying conditions, and printing parameters on printability and mechanical performance were systematically examined. GA showed a higher tap density (0.87 ± 0.01 g/cm³) than rice husks (0.50 ± 0.25 g/cm³), indicating a more compact structure. Printing tests indicated that pastes with particle sizes of 90–125 µm achieved optimal extrusion, characterized by continuous filament deposition, minimal nozzle clogging, and stable geometry at 60 mm³/s. Extrusion energy decreased as binder content increased, reflecting improved material flow. These properties enabled smooth extrusion and effective shape retention following deposition. Printing experiments confirmed that both GA and rice husk particles within the 0 < d < 250 µm range were printable, with the 125 µm < d < 250 µm fraction yielding the most consistent results at flow rates of 40 –72 mm³/s and drying at 45–55 °C for 24 h. Printing experiments confirmed that both GA and rice husk particles within the 0 < d < 250 µm range were printable using a 4 mm diameter Nozzle, with the 125 µm < d < 250 µm exhibited the highest flexural (8.29 ± 0.96 MPa) and compressive strengths (5.05 ± 1.56 MPa) due to effective load transfer and reduced binder demand.

Keywords-additive manufacturing; gum arabic; mechanical properties; rice husk

I. INTRODUCTION

Additive Manufacturing (AM) techniques, including binder jetting and extrusion-based processes, heavily rely on suitable binder systems to ensure the structural cohesion, dimensional fidelity, and functional performance of printed components [1]. Advances in process optimization and monitoring have demonstrated substantial improvements over conventional

approaches, achieving a 10% reduction in material consumption, a 33% decrease in surface roughness, a 22% reduction in production time, and a 98.7% accuracy in defect detection [2].

Cellulose-based binders, such as Methylcellulose (MC), Hydroxypropyl Methylcellulose (HPMC), and Hydroxyethyl Cellulose (HEC), constitute the primary class of conventional bio-based binders in extrusion-based AM [3]. These binders impart shear-thinning properties, enhance green strength, and improve shape retention during extrusion. However, these materials often require high concentrations, are sensitive to water content and processing conditions, and may increase material costs. and complex disposal or recycling routes [4]. Such characteristics limit their alignment with emerging sustainable and green AM paradigms [5], especially in regions where environmental impact, cost, and material availability are crucial constraints. Research on AM has emphasized that the next generation of AM materials systems must integrate bio-based polymers, waste-derived fillers, and recyclable formulations without compromising mechanical performance or print reliability [6].

Sodium Alginate (SA) is used in extrusion-based AM [7] due to its rapid ionic gelation, biocompatibility, and ability to form hydrogels. Alginate-based inks are widely employed in pharmaceutical and bio printing [8], where rheological tuning through polymer concentration, cross-linker content, and blending with other polymers is significant for achieving shape fidelity and mechanical integrity. However, alginate systems often require multicomponent formulations, e.g., calcium salts, secondary polymers, and controlled cross-linking environments [9]. Alginate-based structures also exhibit significant drying shrinkage and brittleness, limiting flexural performance in highly humid or aggressive environments. In addition, commercial SA can be relatively expensive and less readily available than regionally sourced gums in some low- and middle-income countries.

Natural gums and polysaccharides are therefore gaining increasing attention as alternative binders and matrix modifiers in AM because they are renewable, water-processable, and exhibit tunable viscoelastic behavior. Research on biopolymer gums highlights their potential as rheology modifiers, structural binders, and functional components in 3D-printed foods, bio-scaffolds [9], and soft devices.

Gum Arabic (GA), a heterogeneous arabinogalactan polysaccharide covalently linked to protein [10], is attractive due to its high-water solubility, interfacial activity, and film-forming ability [11], which together underpin its performance as both a temporary and functional binder. Its Arabinogalactan Protein (AGP) domains promote strong adsorption and anchoring at solid-liquid interfaces [12], enabling robust particles to bind networks that can sustain cyclic or dynamic loading [13].

Despite these advantages, GAs have rarely been investigated as primary binders for structural bio-based composites in AM. Most reported applications have focused on pharmaceutical formulations, food systems, electrochemical devices, hydrogels, or soft sensors [14], where the load-bearing capacity is not a significant requirement. This lack of application in structural AM is important, as extrusion-based printing of construction, packaging, or composite components demands binder systems that simultaneously provide printability, green strength, and post-print mechanical integrity.

Evidence of GA's binding efficacy is nonetheless well-established in pharmaceutical tableting, where Acacia gums are used as wet-granulation and direct-compression binders [15] capable of producing tablets that meet pharmacopeial friability limits [16], exhibitING acceptable tensile strengths. GA has also been combined with thermoplastic matrices, such as polycaprolactone, or used in Fused Filament Fabrication (FFF) to fabricate drug-loaded dosage forms [17], demonstrating compatibility with powder-bed, melt-based, and extrusion-based AM processes.

Agricultural residues, such as rice husk, are promising fillers and reinforcement phases for sustainable AM. Rice husk is rich in silica and lignocellulose components, widely available as a low-cost by-product of rice milling, and has been incorporated into polymer matrices, such as polylactic acid (PLA), to produce FFF filaments and printed components [18]. Although these studies demonstrate improved stiffness and reduced material cost, they often report reduced toughness and process ability, especially at high filler loadings.

Beyond thermoplastic filaments, rice husk has also been used in earthen and geopolymer-based formulations for 3D-printed construction elements [19], where it serves as both a lightweight aggregate and a crack-bridging fiber. This application underscores the potential of rice husk as a functional, bio-based filler in AM, while also highlighting the need for compatible binder systems to address its low bulk density, irregular morphology, and high porosity.

Previous studies mainly investigated GA as a binder or additive in pharmaceuticals, food, and electrochemical systems. This study instead defines a processing window that ensures stable extrusion, good shape fidelity, and strong interlayer bonding without sacrificing compressive and flexural strength. It is hypothesized that AGP fractions in GA form hydrogen-bonded interfaces with the silica-rich and lignocellulose surfaces of rice husk particles, enhancing polymer bridging, particle cohesion, and load transfer.

By systematically assessing rheology, powder flow, printability, and mechanical performance across different particle sizes, binder ratios, and extrusion conditions, this work demonstrates GA's potential as a fully plant-based, sustainable binder for structurally relevant rice-husk and other bio-based composites in extrusion-based AM.

II. METHODOLOGY

The flow diagram of the proposed methodology is illustrated in Figure 1.

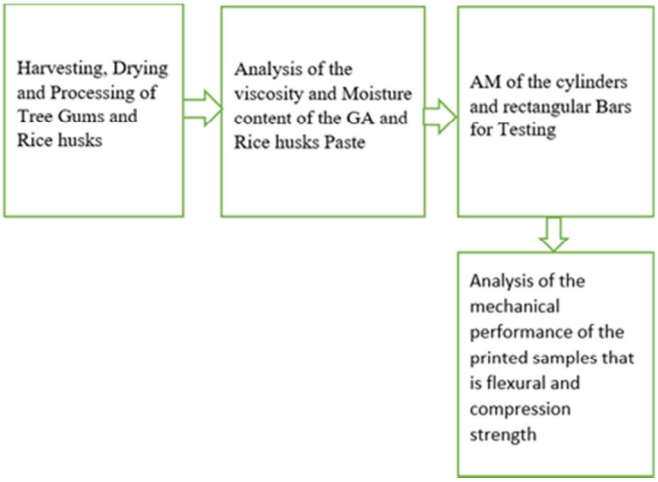

Fig. 1. Methodology flow diagram.

A. Material Preparation

GA and rice husks were selected for paste extrusion due to their compatibility and processing benefits. Rice husks provide low-cost, silica-rich reinforcement, while GA offers natural adhesion, water solubility, and favorable rheology for stable extrusion.

The process began with solar drying of rice husks for 72 hours to prevent clumping and agglomeration during subsequent milling and sieving, and to enhance powder flowability. Rice husks were then chopped into small particles using a hammer mill, followed by further refinement with a ball mill to obtain printable particle sizes below 250 µm, as supported by the literature. Particle size analysis was conducted using a Haver EML Digital Plus sieve shaker (Haver & Boecker, Oelde, Germany) in accordance with ASTM E11. The resulting powders were classified into three size ranges: d <90 µm, 90 µm < d < 125 µm, and 125 µm < d < 250 µm. The complete grinding, milling, and sieving procedure is shown in Figure 2.

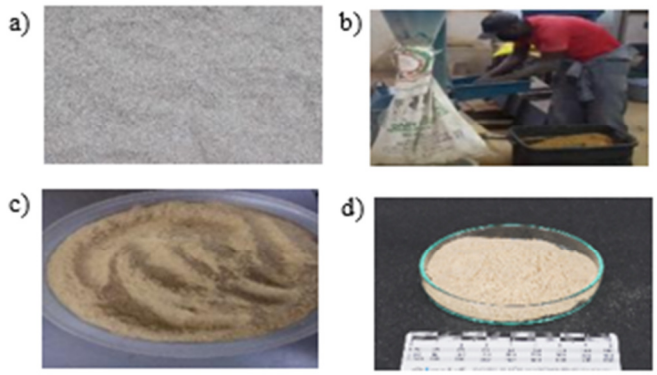

Fig. 2. Processing steps for rice husk powder preparation: (a) raw rice, (b) grinding / milling, (c) milled rice husk powder, and (d) sieved rice husk powder.

GA was dried in a solar dryer for 72 h to further reduce moisture content and improve powder flowability. The material was then milled and sieved, as displayed in Figure 3. The resulting GA samples were evaluated for their rheological and flowability properties.

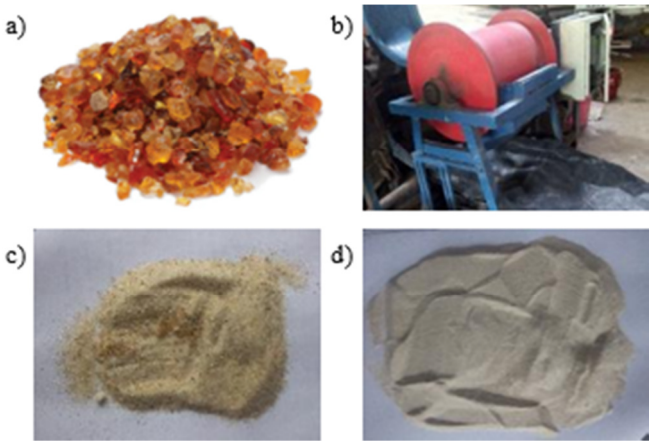

Fig. 3. Processing steps for GA powder preparation: (a) raw GA, (b) milling process, (c) milled powder, and (d) sieved powder0.

B. Powder Characteristics

Bulk and tap densities were measured using a Hall flow funnel and a 250-mL graduated cylinder in accordance with ASTM B213 and USP <616>, respectively. The Hauser ratio and compressibility index were subsequently calculated to evaluate flowability, as illustrated in Figure 4.

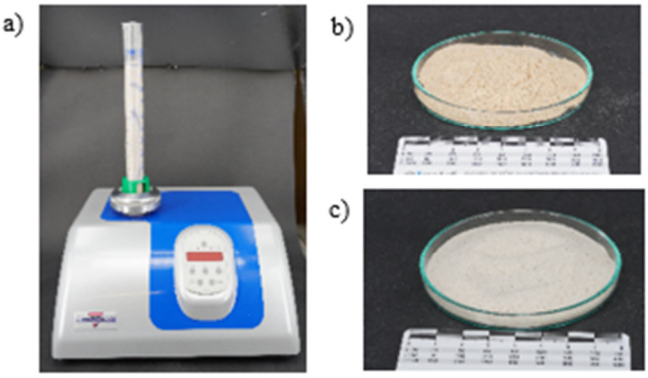

Fig. 4. (a) 100 ml graduated cylinder, (b) rice husks, and (c) GA.

To measure tap density (ρ_t), a 100 ml graduated cylinder containing dried GA and rice husk powder was tapped until readings remained constant across five consecutive sequences. The final volume (Vf) was then recorded. This procedure was repeated three times for each particle size. The tap density was subsequently determined by dividing the mass of the powder before tapping by the minimum volume after tapping.

C. Paste Extrusion Material Preparation

Rice husk and GA powders were mixed in different proportions to form an extrudable paste, as portrayed in Figure 5. This was done for particle sizes below 250 µm, with rice husk powder serving as the filler material and GA as the binder. Treated water was used to prepare the paste. The filler-

to-binder formulas used 7 parts of rice husk powder and 1, 2, and 3 parts of GA powder. The ingredients were mixed in a KLARSTEIN Grand Prix mixer at 600 rpm for 10 min with a multi-blade attachment. Mixing was performed at room temperature (22–25 °C) and 40–60% relative humidity.

Fig. 5. (a) Rice husk + GA + water mixing using the hands and (b) rice husk + GA paste ready for extrusion.

Moisture content measurements across different binder-to-filler ratios and particle-size fractions yielded consistent results, ranging from 51.76% to 55.21%, as depicted in Table I. Increasing particle size decreased moisture content. For instance, at a 7:1 ratio, the 90-µm fraction had a moisture content of 54.87 ± 0.74%, which declined to 52.30 ± 0.16% for the 250-µm fraction. This pattern was also evident for the 7:2 and 7:3 ratios. The elevated moisture content in finer particles is attributed to their greater specific surface area, which promotes water adsorption and binder wetting. Conversely, coarser particles have lower surface area and reduced capillary retention, resulting in slightly lower moisture levels.

TABLE I. MOISTURE CONTENT OF THE RICE HUSKS AND GA PASTE

Ratio	**Moisture content (%M)**		
	90µm	***125µm***	***250µm***
7:1	54.87±0.74	54.15±0.63	52.30±0.16
7:2	55.21±0.41	54.01±0.58	53.03±0.67
7:3	54.63±0.78	53.76±0.45	51.76±0.45

Across the tested binder ratios (7:1, 7:2, and 7:3), moisture content remained stable within each particle size class, suggesting that binder proportion had a secondary effect on moisture retention in this range. For example, in the 125 µm fraction, moisture content values were 54.15 ± 0.63%, 54.01 ± 0.579%, and 53.76 ± 0.45% for the respective ratios. Moisture content was measured using a halogen moisture analyzer (DAB 100-3, KERN & Sohn, Balingen, Germany), which determines moisture content by calculating mass loss during controlled heating. These results demonstrate that particle size is the primary determinant of moisture distribution, with finer fractions retaining more water due to increased surface area and adsorption capacity.

D. Extrudability Test

The samples were prepared at different filler-to-binder ratios, namely 7:1, 7:2, and 7:3, at a room temperature of 22°C, a relative humidity of 36% RH, and a moisture content of 50%M consistently. The samples were covered well and kept in room conditions to allow further bonding between the filler and the binder. Four samples of each filler-to-binder ratio, as well as the reference samples, were pushed through an empty syringe. This helped to determine the net extrusion energy. The samples were tested for extrudability using a universal testing machine at a speed of 5 mm/s [20], as shown in Figure 6.

Fig. 6. Extrusion energy testing.

E. Paste Extrusion

The CAD models for the test specimens were designed to conform to the ASTM standards for the compression testing of the cylinders (Ø20 × 40 mm), and ISO standards for the flexural strength of the rectangular bars (80 × 10 × 4 mm). These models were exported as STL files. The 3D Prusa Slicer 2.9.3 software was employed to slice the models and generate the required G-code for 3D printing. Test samples were fabricated using a modified, in-house FFF system equipped with a syringe-based plunger extrusion mechanism [21].

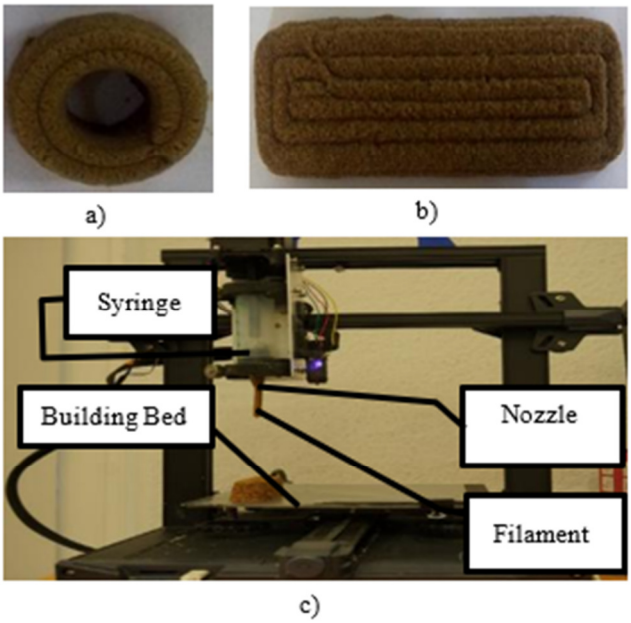

Fig. 7. Printing process: (a) cylinder for compression testing, (b) rectangular bar for flexural testing, (c) paste extrusion machine during printing.

A stepper motor provided steady actuation of the piston, ensuring consistent paste extrusion through a 4 mm-diameter nozzle and achieving controlled flow and repeatable pressure. Cylindrical and rectangular specimens were produced from rice husk–GA pastes using the paste extrusion system at flow rates ranging from 40 mm³/s to 72 mm³/s, with a 4 mm nozzle diameter, as presented in Figure 7.

F. Post-Processing of the Printed Samples

After printing, the samples were exposed to ambient air to facilitate the gradual evaporation of surface moisture, thereby minimizing deformation and cracking. The specimens were then oven-dried at 45–55 °C for 72 h to eliminate residual internal moisture. Drying was deemed complete when consecutive mass measurements differed by less than 0.1%, indicating moisture equilibrium. This protocol stabilized the material structure and ensured consistent, reliable mechanical performance.

G. Compression Strength Testing

Compression testing was conducted to assess the compressive strength and deformation behavior of printed samples under monotonic loading using a universal testing machine, with ASTM D695 serving as the guiding framework. The specimens were positioned between two circular steel plates, one fixed and the other movable, and subjected to displacement-controlled loading at 5 mm/min until failure, with a maximum applied load of 5500 N. The end surfaces of the specimens were tested as printed, without sanding.

H. Bending Testing

Flexural strength was assessed using a three-point bending configuration in accordance with ASTM D790, utilizing rectangular beam specimens. The specimens rested on two lower supports, and a single-point load was applied centrally via an upper loading nose. The load was applied under displacement control until specimen failure, with a maximum force of 250 N. This testing configuration facilitated the evaluation of bending behavior and flexural resistance relevant to structural performance, and the specimens were tested as printed.

Flexural and compression tests were conducted on a Shimadzu Universal Testing Machine (Model ME-8236, Shimadzu Corporation, Kyoto, Japan) at Jomo Kenyatta University of Agriculture and Technology (JKUAT).

III. RESULTS AND DISCUSSION

A. Tap Density and Packing Behavior

GA had a greater mass (78.83 kg) than rice husks (52.12 kg) and a slightly larger volume (90.6 ml vs 83.4 ml), as demonstrated in Table II. As a result, GA exhibited a significantly higher tap density (0.87 ± 0.01 g/cm³), suggesting a more compact, less porous structure. Conversely, rice husks exhibited a lower tap density (0.50 ± 0.25 g/cm³), indicating increased particle irregularity and a higher proportion of interparticle voids.

TABLE II. TAP DENSITY AND PACKING BEHAVIOUR OF GA AND RICE HUSKS

Parameters	GA	Rice husks
Mass (kg)	78.83	52.12
Volume (ml)	90.6	83.4
Tap density (g/cm^3)	0.87 ± 0.01	0.50 ±-0.25

B. Range of Printing Parameters

Printing experiments indicated that rice husk–GA pastes with particle sizes < 250 µm were suitable for extrusion-based printing. The 90-125 µm particle size fraction demonstrated the most reliable extrusion performance, as evidenced by continuous filament deposition, minimal nozzle clogging, consistent filament width, and stable start–stop response, consistent with powder flowability analysis.

In contrast, both the finest (d < 90 µm) and coarsest (125 µm < d < 250 µm) particle size ranges required flow rates above 40 mm³/s, which often led to filament spreading and dimensional deviations from the intended geometry, resulting in increased material wastage.

The increased material wastage observed at higher flow rates results from over-deposition, in which the material delivery rate exceeds both the nozzle movement rate and the paste's self-supporting capacity. In contrast, the 90 µm to 125 µm particle size class yielded well-defined structures at flow rates of 40, 60, and 72 mm³/s. Among these, 60 mm³/s was determined to be optimal, producing minimal dimensional deviation and enhanced surface definition.

Drying was performed at 45–55 °C for 24 h, as temperatures above 60 °C may degrade the internal microstructure and adversely affect mechanical performance. These parameters collectively define a robust processing window for achieving high printability, dimensional fidelity, and surface quality in GA-based paste extrusion.

C. Extrusion Energy

The results indicate a clear and consistent negative relationship between binder level and Unit Extrusion Energy (UEE) when GA is used. Both the regression plot and the averaged data show that increasing the binder level from low (-1) to high (+1) results in a substantial decrease in energy, from approximately 67.7 J/mm to -9.3 J/mm, as shown in Figure 8. A negative UEE indicates that extruding the paste required less energy compared to squeezing an empty syringe.

Linear regression analysis corroborates this trend, with a strong negative slope (-38.54) and a high coefficient of determination (R^2 = 0.948), suggesting that binder level explains most of the variation in extrusion energy, as depicted in Figure 9.

However, despite the apparent strength of this relationship, the effect is not statistically significant (p=0.146). These findings suggest that increasing the binder content enhances the material flow and reduces the extrusion resistance, although further data and validation are required to confirm the statistical robustness of this relationship.

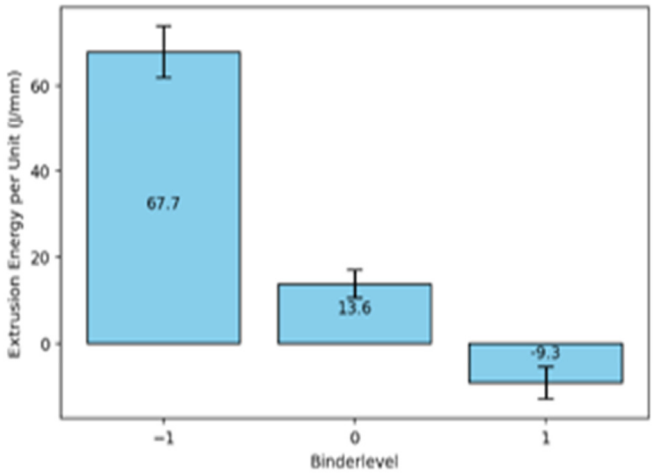

Fig. 8. Extrusion energy of the rice husk + GA paste.

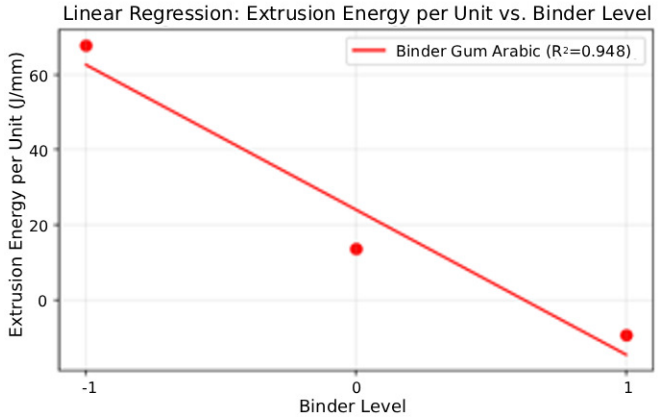

Fig. 9. Linear regression showing the extrusion energy per unit vs binder levels.

D. Mechanical Tests

1) Flexural Strength Tests

For the finest particle size range (>90 µm), flexural performance increases consistently with higher binder content, as displayed in Figure 10. Mixtures with a 7:1 filler-to-binder ratio exhibit a relatively low flexural strength of 2.93 MPa with a standard deviation of 1.36. Increasing the binder to a 7:2 ratio substantially improves strength, yielding 5.66MPa with a standard deviation of 1.23. The highest flexural strength within this particle size class was achieved with a 7:3 filler-to-binder ratio, reaching 6.32 MPa with a standard deviation of 0.726. This result confirms that an additional binder enhances matrix cohesion and load transfer capacity.

Samples with particle sizes between 90 and 125 µm demonstrated a flexural strength of 3.85 MPa with a standard deviation of 0.01 at a 7:1 ratio. This figure increased to 4.41 MPa with a standard deviation of 0.05 at a 7:2 ratio, and rose markedly to 5.43 MPa with a standard deviation of 0.64 at a 7:3 filler-to-binder ratio. These results indicate that this particle class benefits from a balanced binder-to-filler ratio, which facilitates effective particle rearrangement and enhances interlayer adhesion. The very high strength observed at higher flow rates and increased filler-to-binder ratios suggests that this particle size compacts more efficiently at elevated deposition velocity, resulting in a denser, mechanically superior structure.

The largest particle size range (125 µm < d < 250 µm) exhibits the highest flexural strength compared to medium-sized particles, while trends remain consistent with binder-ratio effects observed in other groups. A 7:1 ratio results in the weakest performance, with strengths of 2.02 MPa and a standard deviation of 0.85. Increasing the filler to binder ratio to 7:2 enhances flexural strength to 4.51 MPa with a standard deviation of 0.75. The highest binder ratio (7:3) yields the most robust structures in this group, with flexural strengths of 8.29 MPa and a standard deviation of 0.96.

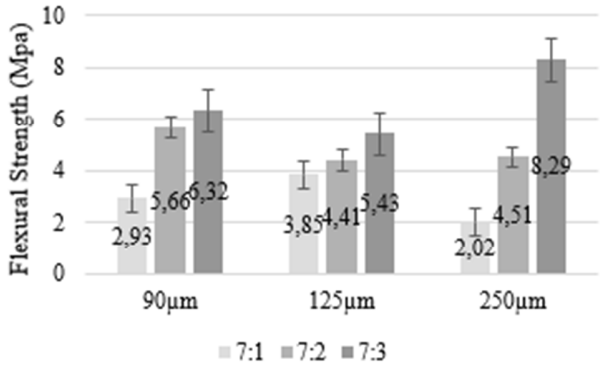

Fig. 10. Flexural strength at different binder ratios and particle sizes.

2) Compression Strength Test

The mechanical performance of the printed samples was significantly influenced by both particle size and the filler-to-binder ratio. Figure 11 demonstrates that the finest particles (d < 90 µm) produced a compression strength of 2.19 MPa with a standard deviation of 1.51 at a 7:1 filler-to-binder ratio. This strength increased to 3.44 MPa with a standard deviation of 1.34 at a 7:2 ratio, and reached 4.24 MPa with a standard deviation of 1.12 at a 7:3 ratio.

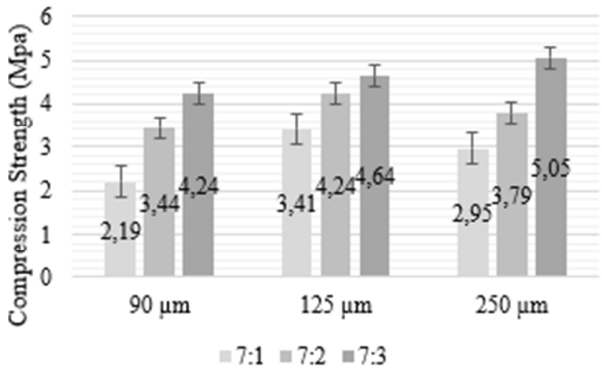

Fig. 11. Compression strength at different binder ratios and particle sizes: < 90 µm, 90 µm < d ≤125 µm and 125 µm < d ≤ 250 µm.

The samples with medium particle sizes (90 < d < 125 µm) exhibited a similar trend: compression strength increased with increasing binder ratio. Specifically, a 7:1 filler-to-binder ratio yielded a compression strength of 3.41 MPa with a standard deviation of 0.96, increasing to 4.24 MPa with a standard deviation of 0.45 at a 7:2 ratio. At a 7:3 filler-to-binder ratio, respectively, the compression strength further increased to 4.46 MPa with a standard deviation of 1.18, highlighting the substantial effect of the binder content on structural integrity.

Finally, samples containing larger particles (125 µm < d < 250 µm) demonstrated the highest mechanical performance. At a 7:1 filler-to-binder ratio, the compression strength was 2.95 MPa with a standard deviation of 0.76, increasing to 3.79 MPa with a standard deviation of 1.56. These findings demonstrate the influence of both filler-to-binder ratios and mixing methods. Formulations with higher binder ratios, especially the 7:3 mixtures, achieved the maximum observed compression strength of 5.05 MPa with a standard deviation of 1.56.

These findings indicate a trade-off between printability and mechanical performance as particle size varies. Particles in the 90 µm < d < 125 µm range exhibited the most reliable extrusion, yielding stable filaments and even layers, resulting in optimal printability. Enhanced processability is a result of improved flowability and homogeneity in pastes with medium-sized particles.

Despite exhibiting superior printability, finer particles did not achieve the highest mechanical strength. Their greater specific surface area increases binder demand during paste preparation, as a significant portion of the binder is consumed in surface wetting rather than forming effective inter-particle bonds. This process limits the formation of a robust load-bearing network within the printed structure.

Conversely, coarser particles measuring 125 µm < d < 250 µm achieved the highest compressive and flexural strengths, recorded at 5.05 MPa (±1.56) and 8.29 MPa (±0.96), respectively. This outcome is attributed to the action of larger particles, which act as rigid aggregates, improving load transfer and preventing crack initiation and propagation, similar to the role of coarse aggregates in conventional concrete. Additionally, their lower surface area reduces binder consumption for wetting, allowing a greater proportion of binder to contribute to inter-particle bonding and overall cohesive strength.

Chemically, increased GA content primarily determines mechanical strength through polysaccharide-silica interactions. Rice husk particles contain amorphous silica with surface silanol groups (Si–OH) [22]. GA, a natural polysaccharide with AGP, has numerous hydroxyl (–OH) groups along its backbone [23]. During paste mixing and extrusion, hydrogen bonds form between the hydroxyl groups of GA and the silanol groups on the rice husk surface. These bonds increase interfacial adhesion between the organic binder and inorganic filler [24].

Increasing binder content supplies more hydroxyl groups and creates a more continuous hydrogen-bonded network [25]. This network strengthens both particle and layer cohesion. Enhanced interfacial bonding enables more effective stress transfer under bending and compressive loads [26]. As a result, mechanical performance improves. Similar hydrogen-bond-driven mechanisms between hydroxyl-rich polysaccharides and silica surfaces have been widely reported [27].

Fracture cross-sections of specimens subjected to compression and bending tests were examined using Scanning Electron Microscopy (SEM). The resulting images reveal a rough, heterogeneous fracture morphology, characterized by flake-like features and embedded filler particles. The fractured surfaces do not exhibit clean particle pullout; instead, matrix remnants are distinctly visible on the particle surfaces.

This morphology indicates that fracture predominantly occurred within the GA binder matrix (cohesive failure) rather than through complete shell–binder interfacial separation. Although localized microvoids and limited interfacial cracking are present, these features are attributed to drying-induced shrinkage and incomplete binder infiltration, rather than adhesive debonding, as shown in Figure 12.

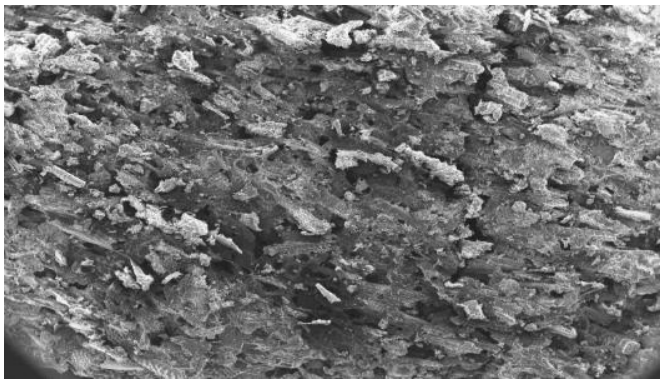

Fig. 12. SEM image for the fractured samples.

The absence of widespread shell detachment and the presence of binder residues adhering to particle surfaces confirm strong interfacial bonding between the shell material and the GA binder. Consequently, the failure mode is primarily cohesive, indicating that the adhesive strength of GA exceeds the internal strength of the binder matrix, and demonstrating its effectiveness as an adhesive under compressive and bending loads.

IV. CONCLUSION

Gum Arabic (GA) is an effective and environmentally sustainable natural binder for rice-husk-based pastes in paste-extrusion Additive Manufacturing (AM). This material demonstrates pronounced shear-thinning behavior, moderate yield stress, and rapid thixotropic recovery. These rheological characteristics facilitate stable extrusion, uniform filament formation, and reliable dimensional stability.

The 90 µm < d < 125 µm particle-size fraction provides the most consistent flowability and extrusion performance. Processing conditions include volumetric flow rates of 40–72 mm^3/s and drying at 45–55 °C for 24 h. Mechanical testing reveals compressive and flexural strengths of up to 5.05 MPa and 8.29 MPa, respectively, at a 7:3 filler-to-binder ratio.

Furthermore, the incorporation of larger particles 125 µm < d < 250 µm enhances load-bearing capacity.

The compressive strength achieved, approximately 5.05 MPa, substantially exceeds that of conventional packaging materials such as expanded polystyrene (0.03–0.30 MPa) and molded pulp (less than 3 MPa). This enhanced performance demonstrates the material's suitability for rigid or semi-rigid packaging applications that require stacking strength and dimensional stability.

Unlike polymer foams, which provide cushioning through elastic deformation, the developed composite exhibits a stiffer mechanical response, making it more appropriate for structural packaging and load-bearing inserts. Collectively, the rheological, printability, and mechanical findings highlight the potential of GA as a natural alternative to synthetic binders in sustainable, bio-based AM.

DECLARATION OF COMPETING INTERESTS

The authors declare no conflicts of interest.

ACKNOWLEDGMENT

This research was supported by the German Federal Ministry of Research, Technology and Space (BMFTR) within the project "RAMMforIU" (Grant No. 01DG25005).

The authors would like to acknowledge the support from the Pan African University for Basic Sciences, Technology, and Innovation (PAUSTI) through the African Union, as well as the "RAMMforIU" project, and a collaboration between Jomo Kenyatta University of Agriculture and Technology (JKUAT) and Technische Universität Bergakademie Freiberg (TUBAF).

DATA AVAILABILITY

The data that support the findings of this study are available from the corresponding author upon reasonable request.

REFERENCES

[1] T. D. Ngo, A. Kashani, G. Imbalzano, K. T. Q. Nguyen, and D. Hui, "Additive manufacturing (3D printing): A review of materials, methods, applications and challenges," *Composites Part B: Engineering*, vol. 143, pp. 172–196, June 2018, https://doi.org/10.1016/j.compositesb.2018.02.012.

[2] N. S. Reddy *et al.*, "Sustainable AI-Driven Hybrid Manufacturing Using Additive and Subtractive Processes," *Engineering, Technology & Applied Science Research*, vol. 15, no. 6, pp. 28878–28884, Dec. 2025, https://doi.org/10.48084/etasr.11785.

[3] A. Gebhardt and J.-S. Hötter, *Additive Manufacturing: 3D Printing for Prototyping and Manufacturing*. Carl Hanser Verlag, 2016.

[4] P. Parandoush and D. Lin, "A review on additive manufacturing of polymer-fiber composites," *Composite Structures*, vol. 182, pp. 36–53, Dec. 2017, https://doi.org/10.1016/j.compstruct.2017.08.088.

[5] M. Shahbazi and H. Jäger, "Current Status in the Utilization of Biobased Polymers for 3D Printing Process: A Systematic Review of the Materials, Processes, and Challenges," *ACS applied bio materials*, vol. 4, no. 1, pp. 325–369, Jan. 2021, https://doi.org/10.1021/acsabm.0c01379.

[6] A. H. A. Hamidie, S. Adzila, A. Razak, and N. M. Isa, "Review of Biopolymer Composite Through 3D Printing Techniques," *Biointerface Research in Applied Chemistry*, vol. 15, no. 1, Feb. 2025, Art. no. 15, https://doi.org/10.33263/BRIAC151.015.

[7] M. Hussein *et al.*, "Investigation of Mechanical Properties of Printed Rice Husk Parts Using an Inhouse Modified Paste Extrusion Printer," in *Sustainable Research and Innovation Conference,* JKUAT Main Campus*,* Kenya, 2023, pp. 14–18.

[8] A. Gholamipour-Shirazi, M.-A. Kamlow, I. T. Norton, and T. Mills, "How to Formulate for Structure and Texture via Medium of Additive Manufacturing-A Review," *Foods*, vol. 9, no. 4, Apr. 2020, Art. no. 497, https://doi.org/10.3390/foods9040497.

[9] E. Yang, S. Miao, J. Zhong, Z. Zhang, D. K. Mills, and L. G. Zhang, "Bio-Based Polymers for 3D Printing of Bioscaffolds," *Polymer Reviews*, vol. 58, no. 4, pp. 668–687, 2018, https://doi.org/10.1080/15583724.2018.1484761.

[10] D. Renard, L. Lavenant-Gourgeon, A. Lapp, M. Nigen, and C. Sanchez, "Enzymatic hydrolysis studies of arabinogalactan-protein structure from Acacia gum: the self-similarity hypothesis of assembly from a common building block," *Carbohydrate Polymers*, vol. 112, pp. 648–661, Nov. 2014, https://doi.org/10.1016/j.carbpol.2014.06.041.

[11] D. Renard *et al.*, "Adsorption of arabinogalactan-proteins from Acacia gums (senegal and seyal) and its molecular fractions onto latex particles," *Food Hydrocolloids*, vol. 125, Apr. 2022, Art. no. 107360, https://doi.org/10.1016/j.foodhyd.2021.107360.

[12] M. Ling *et al.*, "Dual-functional gum arabic binder for silicon anodes in lithium ion batteries," *Nano Energy*, vol. 12, pp. 178–185, Mar. 2015, https://doi.org/10.1016/j.nanoen.2014.12.011.

[13] S. I. Abdelwahab, M. M. E. Taha, and A. A. Mariod, "Performance analysis, conceptual mapping, and emerging trends for Gum Arabic research: a comprehensive bibliometric analysis from 1916 to 2023," *Food Production, Processing and Nutrition*, vol. 7, Jan. 2025, Art. no. 4, https://doi.org/10.1186/s43014-024-00276-y.

[14] M. M. Sarab Badieh *et al.*, "Biological gum-based biopolymers as advanced materials for 3D printing applications: A review," *European Polymer Journal*, vol. 241, Dec. 2025, Art. no. 114212, https://doi.org/10.1016/j.eurpolymj.2025.114212.

[15] K. H. Desta, E. Tadese, and F. Molla, "Physicochemical Characterization and Evaluation of the Binding Effect of Acacia etbaica Schweinf Gum in Granule and Tablet Formulations," *BioMed Research International*, vol. 2021, no. 1, Oct. 2021, Art. no. 5571507, https://doi.org/10.1155/2021/5571507.

[16] G. Auriemma, C. Tommasino, G. Falcone, T. Esposito, C. Sardo, and R. P. Aquino, "Additive Manufacturing Strategies for Personalized Drug Delivery Systems and Medical Devices: Fused Filament Fabrication and Semi Solid Extrusion," *Molecules*, vol. 27, no. 9, Apr. 2022, Art. no. 2784, https://doi.org/10.3390/molecules27092784.

[17] G. Pitzanti, E. Mathew, G. P. Andrews, D. S. Jones, and D. A. Lamprou, "3D Printing: an appealing technology for the manufacturing of solid oral dosage forms," *Journal of Pharmacy and Pharmacology*, vol. 74, no. 10, pp. 1427–1449, Oct. 2022, https://doi.org/10.1093/jpp/rgab136.

[18] M. N. Andanje, J. W. Mwangi, B. R. Mose, and S. Carrara, "Biofilaments from recycled high-density polyethylene and rice husks for fused filament fabrication," *Materialwissenschaft und Werkstofftechnik*, vol. 56, no. 4, pp. 581–600, Apr. 2025, https://doi.org/10.1002/mawe.202400168.

[19] E. Ferretti, M. Moretti, A. Chiusoli, L. Naldoni, F. de Fabritiis, and M. Visonà, "Rice-Husk Shredding as a Means of Increasing the Long-Term Mechanical Properties of Earthen Mixtures for 3D Printing," *Materials*, vol. 15, no. 3, Jan. 2022, Art. no. 743, https://doi.org/10.3390/ma15030743.

[20] A. Fasihi and N. A. Libre, "From pumping to deposition: A Comprehensive review of test methods for characterizing concrete printability," *Construction and Building Materials*, vol. 414, Feb. 2024, Art. no. 134968, https://doi.org/10.1016/j.conbuildmat.2024.134968.

[21] H. Zeidler, L. Micke, L. Kühnel, M. Lamottke, and M. Denker, "Material extrusion printer for pastes based on a commercial desktop filament printer for plastics," in *Open Source Hardware Konferenz,* Dresden, 2024, https://doi.org/10.69558/2024004.

[22] R. K. Iler, *The Chemistry of Silica: Solubility, Polymerization, Colloid and Surface Properties and Biochemistry of Silica*. New York: John Wiley and Sons, 1979.

[23] H. E. Bergna and W. O. Roberts, Eds., *Colloidal Silica: Fundamentals and Applications*. Boca Raton: Taylor & Francis, 2005.

[24] L. T. Zhuravlev, "The surface chemistry of amorphous silica. Zhuravlev model," *Colloids and Surfaces A: Physicochemical and Engineering Aspects*, vol. 173, no. 1–3, pp. 1–38, Nov. 2000, https://doi.org/10.1016/S0927-7757(00)00556-2.

[25] G. Siqueira, J. Bras, and A. Dufresne, "Cellulosic Bionanocomposites: A Review of Preparation, Properties and Applications," *Polymers*, vol. 2, no. 4, pp. 728–765, Dec. 2010, https://doi.org/10.3390/polym2040728.

[26] I. Elfaleh *et al.*, "A comprehensive review of natural fibers and their composites: An eco-friendly alternative to conventional materials," *Results in Engineering*, vol. 19, Sept. 2023, Art. no. 101271, https://doi.org/10.1016/j.rineng.2023.101271.

[27] K. Y. Lee and D. J. Mooney, "Alginate: Properties and biomedical applications," *Progress in Polymer Science*, vol. 37, no. 1, pp. 106–126, Jan. 2012, https://doi.org/10.1016/j.progpolymsci.2011.06.003.